2008

The Role of Diffusive Transport on Low and Intermediate Temperature Hydrocarbon Oxidation: Closed Reactor Experiments using Equimolar n-Butane + Oxygen Premixtures at Reduced-Gravity

Howard Pearlman
Drexel University

Michael R. Foster
George Fox University, mfoster@georgefox.edu

THE ROLE OF DIFFUSIVE TRANSPORT ON LOW AND INTERMEDIATE TEMPERATURE HYDROCARBON OXIDATION: CLOSED REACTOR EXPERIMENTS USING EQUIMOLAR $n-C_4H_{10}+O_2$ PREMIXTURES AT REDUCED-GRAVITY

Howard Pearlman* **and Michael Foster**

Drexel University, Department of Mechanical Engineering and Mechanics, Philadelphia, Pennsylvania

Experiments were conducted in a closed, spherical reactor aboard NASA's KC-135 reduced-gravity aircraft using an equimolar $n-C_4H_{10}+O_2$ premixture ($Le = 1.3$) at subatmospheric pressures to compliment model predictions and further explore the reactive-diffusive structure of cool flames and ignitions. The pressure and radial temperature histories were recorded and analyzed for different initial conditions. In addition, the visible light emission from excited formaldehyde was recorded using an intensified video camera and was observed to be radially symmetric in all cases. Unexpectedly, however, the measured temperature distributions during (and after the passage of) the cool flames and ignitions were not parabolic as predicted by conduction models, which suggests the onset of weak convection at 10^{-2} g.

Keywords: Cool flames; Microgravity; Reaction-diffusion; Static reactor; Two-stage ignition

INTRODUCTION

Using free-fall facilities (e.g., drops towers, aircraft, space-based platforms) to reduce the effective gravitational acceleration, natural convection can be suppressed in non-isothermal combustion studies. Drop towers offer 2.2 to 5.0 s of reduced-gravity time at 10^{-4} to 10^{-5} g, while aircraft (including NASA's KC-135 and ESA's Airbus A-300) can provide 20 s of test time by freely-falling approximately 2440 m (8000 ft, from 32 kft to 24 kft) at 10^{-2} g. Note, the g-level in the aircraft are 2 to 3 orders of magnitude larger due to mechanical and aerodynamic-induced vibration. Space-based facilities are the ideal facility for such experiments as they can achieve near-zero gravity (10^{-5}–10^{-6} g) for weeks or months, yet access is prohibitively expensive and limited.

The objective of this study is to report the pressure histories, the temperature distributions, and the recorded visible images associated with cool flames and

Special thanks are extended to Ming-Shin Wu, Richard Chapek, Donna Neville, and Scott Numbers at NASA GRC for programmatic and flight support for the microgravity experiments. This work was funded by NASA under grant NCC3-1006. The authors acknowledge financial support for MF from the NSF Graduate Research Fellowship Program.

*Address correspondence to hp37@drexel.edu

multi-stage ignitions observed in closed reactor experiments conducted aboard NASA's KC-135 aircraft. All experimental data reported herein was obtained using an equimolar $n-C_4H_{10}+O_2$ premixture in a 10 cm diameter spherical, closed reactor. As noted, the intent was to suppress convection and thereby reduce the associated Rayleigh number ($Ra = Gr\ Pr = \beta g \Delta T R^3/\nu\alpha$) below the critical value for onset of convection, $Ra_{cr} \approx 600 \pm 400$ (Tyler, 1966; Fine et al., 1970; Barnard and Harwood, 1974).

In our 10 cm diameter spherical, static reactor, computed values of the Ra range from 8×10^4 to 1×10^5 at terrestrial conditions for an equimolar $n-C_4H_{10}+O_2$ premixture assuming a representative temperature rise of 100 K for cool flames. These values are based on mixture-averaged property values computed in the temperature range from 570 to 630 K and sub-atmospheric pressures from 60 to 70 kPa. Thus, the values of the Ra aboard the aircraft are expected to be in the range of 800 to 1000, which are within the experimental error bar on the reported value of Ra_{cr} (Tyler, 1966; Fine et al., 1970). If, however, the temperature excess significantly exceeds 100 K, as in ignition studies, natural convection will likely not be effectively suppressed at 10^{-2} g. For these cases, facilities capable of achieving lower gravity-levels or perhaps high levels of inert dilution are needed to maintain $Ra < Ra_{cr}$.

APPARATUS

The apparatus used for all experiments was described in our prior work (Foster and Pearlman, 2006, 2007) and consisted of a spherical fused-silica reactor (10.2 cm internal diameter, 3 mm wall thickness) housed in an isothermal furnace monitored with two type-K thermocouples (reported accuracy: ±2.2°C). The reactor was initially cleaned with a dilute solution of ammonium bifluoride and thoroughly rinsed with deionized water and dried. Prior to the experiments, the reactor was preheated to the desired temperature (573–623 K) and evacuated to 2.7×10^{-3} kPa (or below) through a single gas entry-exit port (25 cm long, 6 mm internal diameter fused-silica tube) using an Edwards GVSP30A dry scroll pump. Each test began during the aircraft ascent, prior to the free-fall portion of the parabolic trajectory, as a pre-evacuated 50 cc 316 stainless-steel cylinder was filled to a prescribed initial pressure with an equimolar mixture of $n-C_4H_{10}+O_2$ (Le = 1.3).

The mixture was prepared prior to flight by partial pressure mixing and stored in one of four 300 cc 316 stainless-steel sample cylinders housed in a gas delivery system that was brought onboard the aircraft. As the plane entered free-fall, as verified with a three-axis Crossbow ±2 g accelerometer mounted on the frame of the furnace, the vacuum pump was isolated from the reactor by closing a manual bellows hand valve. The reactor was then filled by opening a pneumatic valve, which allowed the premixture stored in the 50 cc cylinder to flow into the reactor. The reactor was then isolated when the pressure equilibrated as determined by a 0–172 kPa Setra™ Model 204 pressure transducer (accuracy: ±0.193 kPa, sample rate: 100 Hz) situated at the inlet to the reactor on the cold side of the furnace. The internal reactor pressure was then monitored using this transducer.

The radial temperature distribution within the reactor was also measured using five type-K thermocouples (bead diameter = 0.71 ± 0.03 mm) inserted along a

horizontal radius through the gas entry-exit port. Thermocouple (TC1) was situated at the center of the reactor and the other thermocouples (TC2–TC5) were positioned 1.29 (±0.01) cm apart. All thermocouples were butt-welded with an exposed bead made from 0.508 mm diameter chromel and alumel wires. From the manufacturer, the advertised response time was 1.5 ± 0.5 s (defined as the time to 63.2% of the actual temperature when subjected to an instantaneous temperature change starting from room temperature air at atmospheric pressure in a 19.8 m/s flow) (Omega Engineering, 2006). Since conduction, rather than convection, is the governing heat transfer mechanism between the reacting gas and the thermocouple at reduced-gravity, the advertised response times cannot be applied. To get a estimate of the actual response time, the time-dependent heat conduction equation was then solved in spherical coordinates (neglecting radiation) for a 0.71 mm diameter Type K chromel thermocouple bead immersed in an equimolar premixture of $n-C_4H_{10}+O_2$ at 50.7 kPa to determine the response time for the microgravity case (details provided in Appendix A).

The computed response time was determined to be 2.8 s. Regardless, the residence times of the reaction fronts (e.g., cool flames) in the vicinity of the thermocouple beads were recognizably shorter than the thermocouple response time and therefore the measured temperature histories underestimate the actual gas temperatures and are taken to be qualitative measurements and can only provide data on the relative changes. Note that these thermocouples, while large, were chosen for their structural integrity at elevated and transient gravity levels at the expense of their response times. For imaging, an intensified Hamamatsu video camera (Model C5909) operating at maximum gain and 30 fps, recorded the reaction through three parallel 3.2 mm thick, 6.4 cm diameter quartz windows mounted in the side-wall of the furnace and spaced 1.27 cm apart to minimize heat loss. The camera was unfiltered, equipped with a quartz lens and has an advertised spectral response between 185–850 nm with excellent sensitivity throughout the visible range (note, excited formaldehyde from cool flames has a strong band near 408 nm; Kondratiev, 1935).

As in all static reactor tests, thermal and pressure equilibration must be established within a fraction of the first induction period to ensure that the initial conditions are well established (Barnard and Harwood, 1974). From the pressure history data, pressure equilibration occurred approximately 2 s after the injection of the reactants. Thermal equilibration occurred in less than 5 s as determined from temperature measurements made with a 0.005 inch diameter type-K thermocouple positioned at the center of the reactor using a non-reactive equimolar $n-C_4H_{10}+N_2$ 2 premixture injected into the preheated vessel at pressures ranging from 13.8 to 65.5 kPa.

RESULTS

Temperature and Pressure Histories

Modes of (a) slow reactions, (b) single cool flames, (c) two-stage ignitions, and (d) single-stage ignitions were observed at reduced-gravity. Representative pressure and temperature histories are shown in Figures 1a–1d for modes (a)–(d) along with the corresponding radial temperature distributions taken from the same data plotted

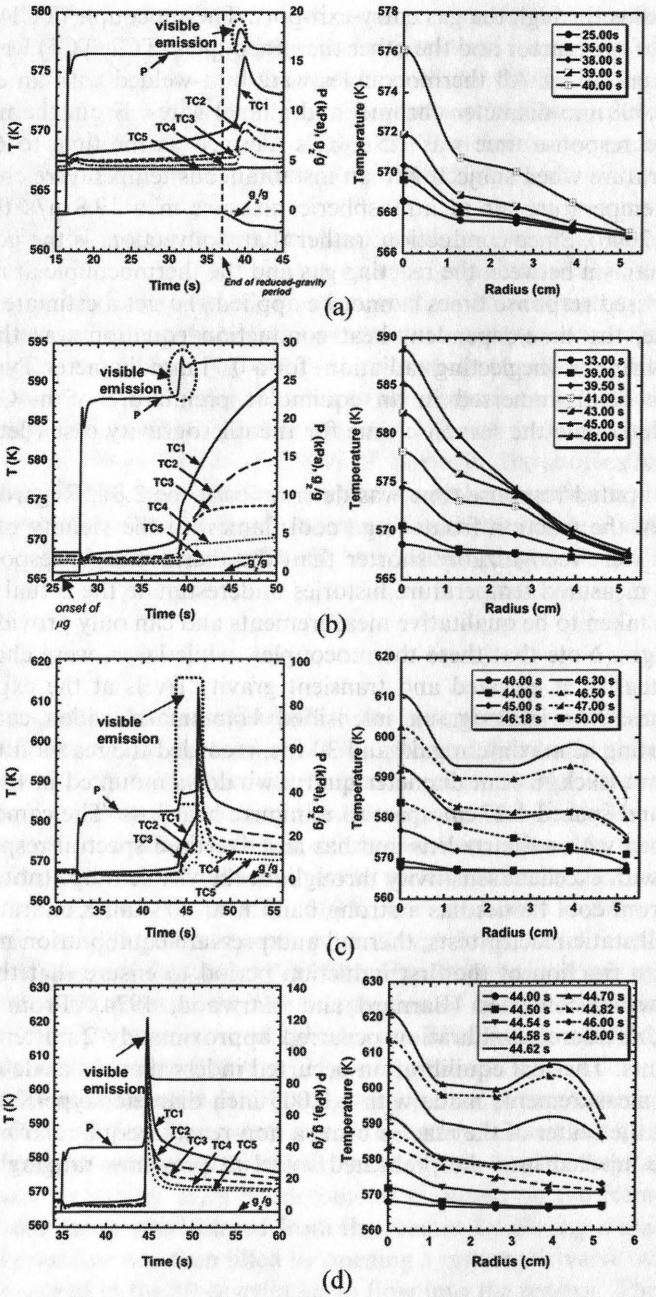

Figure 1 Left side: The pressure history (P), the radial temperature distribution (g_z, —T1 - - -T2 -----T3 ·····T4 -----T5), and the vertical component of acceleration normalized by Earth's gravitational acceleration (g) for representative modes that include: (a) slow reaction (T = 568 K; P = 15.9 kPa), (b) cool flames (T = 568 K; P = 22.7 kPa), (c) two-stage ignition (T = 568 K; P = 31.7 kPa) and (d) single-stage ignition (T = 568 K; P = 40.3 kPa). Right side: The radial temperature distribution plotted at different times. The distributions indicated by the dashed lines represent the temperature decay as the gas cools. All thermocouple measurements have an accuracy of ±2.2°C (Omega Engineering, 2006).

at different times. Note that the initial time in all plots is arbitrary and simply corresponds to the time from the start of the data acquisition system to the injection of the reactants.

For the case shown in Figure 1a, the initial pressure was 15.9 kPa and the pressure and temperature increase after 20 s was 0.3 kPa and 2°C (within the experimental accuracy of the thermocouple). No visible light emission was detected during this period. However, at the end of the available reduced-gravity test time (i.e., the free-fall portion of the parabolic flight), the aircraft accelerated upwardly in preparation for another free-fall maneuver as indicated in the acceleration profile. During this transient period, a cool flame developed in the upper half of the reactor (suggesting the onset of convection) at $t = 38$ s accompanied by a 2.1 kPa pressure increase.

Tests at lower pressures displayed similar behavior, showed little or no evidence of reaction during the available test time, and no evidence of a cool flame or significant reaction after the reduced-gravity test period. Note that the radial temperature distribution is likely not parabolic due to the onset of natural convection. Rather, the temperature achieved a maximum at the center, decayed to a plateau and then cooled to the wall temperature.

For pressures ranging from 10 to 35 kPa and initial temperatures less than 623 K (see ignition diagram below, Figure 4b), single cool flames were observed. For the case shown in Figure 1b, the pressure increased $\sim$8 kPa and visible light emission was observed for the period indicated. Figure 2 shows the light emission for a cool flame at a slightly higher temperature. As in previous studies, the cool flame started at the center and propagated radially outward, apparently unaccompanied by natural convection. Examination of the radial temperature history, however, shows that the temperature profile is not nearly parabolic as expected from a pure conduction model. Rather, the temperature increased most rapidly at the center, reached a plateau in the central region and decayed to the wall temperature during and shortly after the observed light emission. Such behavior suggests the existence of weak convection.

As mentioned before, the Ra is less than the Ra_{cr} if the maximum temperature rise remains less than 100°C at 10^{-2} g. From Figure 1b, the peak measured temperature rise is $\sim$20°C. For the actual temperature rise to remain below 100°C, a conductive heat transfer analysis was developed, assuming constant thermal properties and a spherical thermocouple bead (shown in the Appendix). From the analysis,

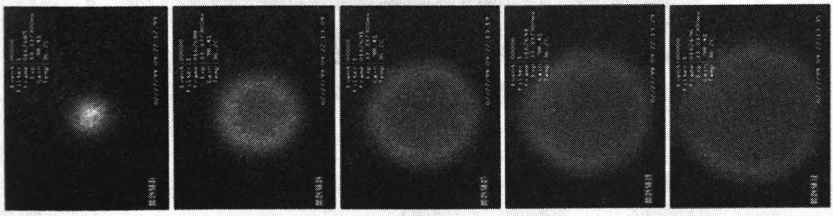

Figure 2 A cool flame at 583 K and 22.1 kPa at reduced-gravity. Time between consecutive frames is 1/30 s.

the nondimensional temperature history, $\theta(t)$, of the thermocouple was numerically computed. The actual temperature rise can then be estimated from the computed temperature history with an estimate of the residence time of the cool flame at the thermocouple. Based on scaling analysis, the residence time can be shown to be the ratio of the thermal diffusivity of the mixture to the square of the average cool flame propagation speed.

In nearly all cases, the cool flame speeds ranged from 2 to 10 cm/s, determined by tracking the peak light emission from the video record, and the thermal diffusivity of the equimolar mixture at 568 K and 22.7 kPa is 1.2 cm^2/s. Thus, the thermal thickness of the flame ranges from 0.12 to 0.6 cm and the corresponding residence times range from 0.01 to 0.3 s. Nondimensionalizing the average time ($t = 0.15$ s) for the thermocouple used, the computed value for $\theta = 0.08$, where θ is the measured temperature difference relative to the actual temperature difference. Since the measured value of $\theta \approx 20/100 = 0.2$, the actual temperature rise is estimated to be ($=20°C/0.08$) 250°C, in which case, the Ra would exceed Ra_{cr} by roughly a factor of 2. A word of caution, however, is needed since the residence time estimates are based on scaling analysis and conduction heat loss along the thermocouple wire leads is neglected in the response time analysis.

At higher reactor pressures, two-stage ignition was also observed. Figure 1c shows a representative data set. Figure 3 shows a typical record of the visible light emission. Interestingly, the cool flame and ignition kernel both started at the center of the reactor and propagated radially outward, while the temperature distribution developed an interesting plateau for radial positions between the center and the wall. Instead, the temperature initially decayed monotonically in the early stages of the cool flame development at the same time a high temperature region developed near the reactor wall ($r \approx 4$ cm). The temperature continued to increase throughout the reactor until 46.3 s (after the ignition event) at which time it then began to cool. Understandably, the slow thermocouple response was unable to quantitatively capture the ignition event. For $t > 46.3$ s, the gas cooled and the peak temperature near the wall decreased more rapidly than at the center due to enhanced conduction heat

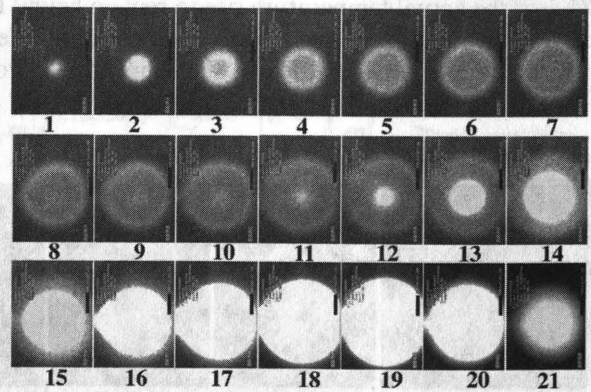

Figure 3 A two-stage ignition at 583 K and 31.7 kPa at reduced-gravity. Time between consecutive frames is 1/30 s.

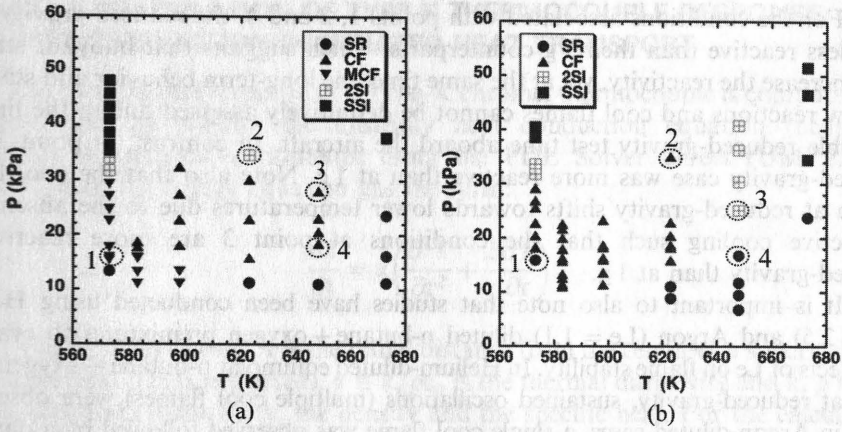

Figure 4 Ignition diagrams at (a) terrestrial conditions and at (b) reduced-gravity for an equimolar premixture of $n-C_4H_{10}+O_2$. SR: slow reaction, CF: cool flames, MCF: multiple cool flames, 2SI: two-stage ignition, SSI: single-stage ignition.

loss to the wall. Interestingly, the visible record showed no evidence of a convective flow as manifest by a lack of radial symmetry.

For higher temperatures and pressures (shown in Figure 4), single-stage ignition was observed as shown in Figure 1d. Similar to ignition stage shown in Figure 3, a high temperature region developed near the reactor wall, yet 30 fps was inadequate to adequately capture the ignition event.

Ignition Diagrams

Ignition diagrams that summarize the modes of reaction observed at terrestrial (1g) and reduced-gravity are shown in Figures 4a and 4b, respectively, for pressures in the range of 6 to 52 kPa and temperatures in the range of 570 to 673 K. The most important finding is that the tests at reduced-gravity are less reactive than their terrestrial counterparts for some conditions, yet more reactive for others. For most of the conditions considered, single or multiple cool flames were observed at 1 g and single cool flames were observed at reduced-gravity. Near stability boundaries, clear differences were observed. Four points are highlighted for comparison and their respective modes of reaction are summarized in Table 1.

Table 1 Comparison between terrestrial (1 g) and reduced-gravity cases highlighted in Figure 4

Points labeled in ignition diagrams	Terrestrial (1 g)	Reduced-gravity
1	Multiple cool flames	Slow reaction
2	Two-stage ignition	Single cool flame
3	Single cool flame	Two-stage ignition
4	Single cool flame	Slow reaction

For the conditions associated with points 1, 2 and 4, the reduced-gravity tests were less reactive than their 1 g counterparts, which suggests that buoyant stirring may increase the reactivity, yet at the same time, the long-term behavior and stability of slow reactions and cool flames cannot be definitively assessed due to the limited available reduced-gravity test time aboard the aircraft. In contrast, at point 3, the reduced-gravity case was more reactive than at 1 g. Note also that the cool flame region at reduced-gravity shifts towards lower temperatures due to the absence of convective cooling such that the conditions at point 3 are more reactive at reduced-gravity than at 1 g.

It is important to also note that studies have been conducted using Helium (Le = 2.5) and Argon (Le = 1.1) diluted n-butane + oxygen premixtures to evaluate the effects of Le on flame stability. In Helium-diluted equimolar n-butane + oxygen mixtures at reduced-gravity, sustained oscillations (multiple cool flames) were observed, while in Argon-diluted cases, a single cool flame was observed followed by a damped oscillatory reaction (Pearlman, 2007). Thus, increasing Le promotes oscillatory cool flames as enhanced conductive heat transfer to the wall (relative to the spatial redistribution of chemical energy owing to diffusive fluxes) cools the reaction to a sufficient extent such that cool flame oscillations are sustained.

CONCLUSIONS

Modes of slow reaction, cool flames, two-stage ignition and single-stage ignition have been observed in a closed reactor at reduced-gravity at temperatures less than 674 K using an equimolar n-butane + oxygen premixture. The pressure histories, visible light emission and radial temperature distribution are reported during the course of the reaction. The temperature distribution associated with representative cool flames was qualitatively similar to that predicted by pure conductive global (i.e., the Wang-Mou model reported in this volume (Pearlman et al., 2008) and the Gray-Yang model (Fairlie et al., 2000; Foster and Pearlman, 2006) model) and that computed using a reduced kinetic mechanism for propane + oxygen cool flames (Figure 6; Fairlie et al., 2004).

As noted, the temperature profile associated with cool flames developed a plateau at intermediate radial locations during and shortly after the visible cool flame. At later times, the reaction continued (non-visibly) and the thermal plateau faded. Such a non-parabolic distribution suggests that natural convection may not be completely suppressed at 10^{-2} g. From the radially symmetric visible light emission, however, the reaction appears to be convection-free. Note that the Ra is $>\mathrm{Ra}_{cr}$ for a temperature excess $\geq 100°C$.

The temperature distribution associated with the two-stage and single-stage ignitions was also non-monotonic and suggest a buoyant recirculating flow (upwardly in the center and downwardly along the walls). This is not unexpected since ignition is accompanied by significant temperature excursions. Again, the interesting dichotomy was that the light emission associated was radially-symmetric as shown in Figure 3, which is not indicative of a buoyant flow. Future studies on the flow field together with fast-response thermocouple measurements will be conducted to further resolve the reactive-diffusive structure.

APPENDIX: CALCULATION OF TYPE-K THERMOCOUPLE RESPONSE TIME FOR CONDUCTION-DOMINATED HEAT TRANSPORT

The temperature response of a Type-K chromel thermocouple is computed as a function time by solving the unsteady heat conduction equation (neglecting radiation) in spherical coordinates using the PDE Solver Direct (UMFPACK) (Davis, 2004); the energy equation has the form:

$$\frac{\partial T}{\partial t} = \alpha\left(\frac{\partial^2 T}{\partial r^2} + \frac{2}{r}\frac{\partial T}{\partial r}\right)$$

where T is the temperature, r is the radial distance from the center of a spherical thermocouple bead (leads neglected), $\alpha \equiv k/\rho c_p$ is the thermal diffusivity and k, ρ and c_p are the thermal conductivity, the density and the specific heat. For the calculation, the diameter of the thermocouple was 0.71 mm, the size used in the experiments. The equation was then solved using the thermocouple properties for $r < 0.355$ mm and gas properties for $r > 0.355$ mm. The heat fluxes are matched at $r = 0.355$ mm, i.e., $k_{TC}(\partial T_{TC}/\partial r) = k_{gas}(\partial T_{gas}/\partial r)$. Also, at $r = 0$, a no heat flux boundary condition was applied and as $r \to \infty, T \to T_{gas}$.

The thermocouple properties were assumed to be constant; the density, specific heat and thermal conductivity are $\rho_{TC} = 8730\,kg/m^3$, $c_{p,TC} = 447.7\,J/kg\cdot K$ (@ 20°C), and $k_{TC} = 19.25\,W/m^2\cdot cK$ (@ 100°C) (Chen et al., 1975). The reactants were equimolar $n\text{-}C_4H_{10} + O_2$ at 50.7 kPa ($\frac{1}{2}$ atm) pressure and assumed to be initially quiescent. With respect to the mixture properties, the values were evaluated at 800 K and 1000 K from experimental correlations (Smith et al., 1960; Touloukian et al., 1970; Chen et al., 1975; DIADEM, 2003).

At 800 K, $k_{mixture} = 0.080\,W/m\cdot K$, $c_{p,mixture} = 2266\,J/kg\cdot K$, $MW_{mixture} = 45.06\,kg/kmol$ and the average $\rho_{mixture} = 0.34\,kg/m^3$ (thus, $\alpha_{mixture} = 1.04\,cm^2/s$).

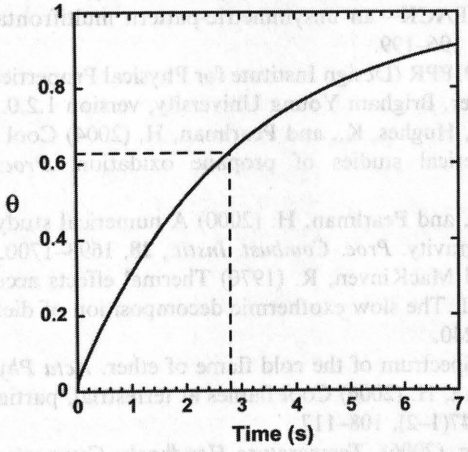

Figure 5 Non-dimensional temperature history for a Type-K chromel thermocouple with a bead diameter = 0.71 mm.

At 1000 K, $k_{mixture} = 0.106\,W/m \cdot K$, $c_{p,mixture} = 2503\,J/kg{\cdot}K$, $MW_{mixture} = 45.06\,kg/kmol$ and the average $\rho_{mixture} = 0.27\,kg/m^3$ ($\alpha_{mixture} = 1.57\,cm^2/s$).

Figure 5 shows the nondimensional temperature ($\theta \equiv \frac{T - T_{TC,initial}}{T_{gas,initial} - T_{TC,initial}}$) history. At t = 0, $\theta_{TC} = 0$ and as the thermocouple temperature approaches the gas temperature, $\theta_{TC} \rightarrow 1$. The response time, i.e., the time to 62.3% rise, is 2.8 s.

NOMENCLATURE

Ra	Rayleigh number
Ra_{cr}	critical Rayleigh number for onset of natural convection
Gr	Grashof number
Pr	Prandtl number
β	coefficient of thermal expansion (K^{-1})
g	Earth's gravitational acceleration (m/s^2)
g_z	gravitational acceleration (m/s^2)
Le	Lewis number based on the deficient component
ΔT	temperature rise (K)
R	characteristic vessel size (radius, m)
P	pressure (kPa)
T	temperature (K)
ν	kinematic viscosity of the mixture (m^2/s)
α	thermal diffusivity of the mixture (m^2/s)

REFERENCES

Barnard, J. and Harwood, B. (1974) Physical factors in the study of the spontaneous ignition of hydrocarbons in static systems. *Combust. Flame*, **22**, 35–42.

Chen, S., Wilhoit, R., and Zwolinski, B. (1975) Ideal gas thermodynamic properties and isomerization of n-butane. *J. Phys. Chem. Ref. Data*, **4**(4), 859–869.

Davis, T. (2004) UMFPACK—an unsymmetric-pattern multifrontal method. *ACM Trans. Math. Soft.*, **30**(2), 196–199.

DIADEM (2003) The DIPPR (Design Institute for Physical Properties) Information and Data Evaluation Manager, Brigham Young University, version 1.2.0.

Fairlie, R., Griffiths, J., Hughes, K., and Pearlman, H. (2004) Cool flames in space: Experimental and numerical studies of propane oxidation. *Proc. Combust. Instit.*, **30**, 1057–1064.

Fairlie, R., Griffiths, J., and Pearlman, H. (2000) A numerical study of cool flame development under microgravity. *Proc. Combust. Instit.*, **28**, 1693–1700.

Fine, D., Gray, P., and MacKinven, R. (1970) Thermal effects accompanying spontaneous ignitions in gases II. The slow exothermic decomposition of diethyl peroxide. *Roy. Soc. Lond.*, **A316**, 223–240.

Kondratiev, V. (1935) Spectrum of the cold flame of ether. *Acta Phys. Chim. URSS*, **4**, 566.

Foster, M. and Pearlman, H. (2006) Cool flames at terrestrial, partial and near-zero gravity. *Combust. Flame*, **147**(1–2), 108–117.

Omega Engineering, Inc. (2006). *Temperature Handbook: Comparison of Time Constant Vs. Overall Outside Diameter of Bare Wire Thermocouple Wires Or Grounded Junction Thermocouples In Air*. Section Z, 51.

Pearlman, H. (2007) Multiple cool flames in static, unstirred reactors under reduced gravity and terrestrial conditions. *Combust. Flame*, **148**(4), 280–284.

Pearlman, H. and Foster, M. (2008) The role of diffusive transport on low and intermediate temperature hydrocarbon oxidation-numerical simulations using the Wang-Mou mechanism. *Combust. Sci. Technol.*, **180**(1), 206–217.

Smith, W., Durbin, L., and Kobayashi, R. (1960) Thermal conductivity of light hydrocarbons and methane-propane mixtures at low pressures. *J. Chem. Eng. Data*, **5**, 316.

Touloukian, Y., Kirby, R., Taylor, R., and Lee, T. (1970) Thermophysical Properties of Matter 13, IFI/Plenum, New York, Washington.

Tyler, B. (1966) An experimental investigation of conductive and convective heat transfer during exothermic gas phase reactions. *Combust. Flame*, **10**, 90–91.